

MOLECULAR ASPECTS ON THE DISSOLUTION AND NUCLEATION OF IONIC CRYSTALS IN WATER

HITOSHI OHTAKI

Coordination Chemistry Laboratories, Institute for Molecular Science,
Okazaki 444, Japan

- I. Introduction
- II. Molecular Dynamic Simulations
 - A. Water-Water Interactions
 - B. Ion-Water Interactions
 - C. Ion-Ion Interactions
 - D. Boundary Conditions
 - E. Procedure of the MD Simulations
 - F. Potential Functions
 - G. Pair Correlation Function and Running Coordination Number
- III. The Solution X-Ray Diffraction Method
 - A. Functions Used for the Diffraction Studies
 - B. Procedures of the X-Ray Diffraction Experiments
- IV. The Dissolution Process of Rock-Salt-Type Alkali Halide Crystals
 - A. Alkali Fluorides
 - B. Alkali Chlorides
 - C. Effects of Masses and the Crystal Faces
 - D. Dissolution Mechanisms
- V. Nucleation Processes of Alkali Halide Crystals
- VI. Molecular Approaches to Crystal Formation and Growth
 - A. Why Do $\text{CoCl}_2 \cdot 4\text{H}_2\text{O}$ Crystals Form Very Slowly and $\text{CoCl}_2 \cdot 2\text{H}_2\text{O}$ Crystals Readily Convert to $\text{CoCl}_2 \cdot 6\text{H}_2\text{O}$ upon Cooling?
 - B. Why Is the Hydrate Melt of $\text{CaCl}_2 \cdot R\text{H}_2\text{O}$ with $R = 6$ Easily Supercooled but Hydrate Melts with $R = 4$ and 8.6 Are Not?
 - C. Why Does the $\text{M}^{\text{I}}\text{Cl} \cdot \text{MgCl}_2 \cdot 6\text{H}_2\text{O}$ Double Salt Form by the Addition of a Small Amount of Alkali Metal Ions M^{I} to a Magnesium(II) Chloride Solution but Not in the Reverse Case?
- VII. Concluding Remarks
- References

I. Introduction

Crystals are beautiful. Many chemists have been attracted by the beautiful color, shape and symmetrical molecular arrangement of crys-

tals, with the result that the chemistry of crystal growth and the study of crystal structures have become an attractive as well as important field of science.

The origin of a crystal is still mysterious. Crystals are formed in the gas, solid, and solution phases, but the majority of crystals are formed in solution. It is generally believable that molecules and ions first gather to form nuclei in supersaturated solution and then grow to macroscopic crystals by collecting around the nuclei. However, no one has ever seen the nucleus of a crystal in solution.

The dissolution of crystals is a well-known phenomenon. It has sometimes been misunderstood that the reaction is the reverse of the deposition process, but this is only true for a saturated solution in equilibrium with crystals.

A number of macroscopic observations have been carried out on crystal formation and dissolution in various solvents by the use of optical and electron microscopes. The kinetic and dynamic properties of crystal growth and dissolution have been investigated in various chemical contexts. The structural analysis of crystals is an indispensable method in chemistry. However, it is still difficult or even impossible to answer the question how a crystal is born.

Another question may arise concerning the dissolution of crystals. For example, when a NaCl crystal is dropped into water, it dissolves. How do we decide which ion in the crystal dissolves first?—a sodium ion or a chloride ion? What is the second ion?—and then the third one? Answers to such questions cannot be derived from macroscopic observations. However, computer simulation techniques may provide some suggestions in answering such questions.

This chapter attempts to review the microscopic mechanism of the dissolution and nucleation processes of crystals at a molecular level with the help of molecular dynamic (MD) simulations and, partly, of solution X-ray diffraction salts. Different procedures are outlined in what follows.

II. Molecular Dynamic Simulations

The reliability of results obtained by molecular dynamic simulations strongly depends on the pair-potential functions employed. If molecules are not strictly spherical, the choice of structure models for the molecules becomes an essential factor determining the reliability of results. A brief discussion of various models will be given. Also discussed are the electron distribution within a water molecule and potential functions

between water molecules, between a water molecule and an ion, and between ions.

A. WATER-WATER INTERACTIONS

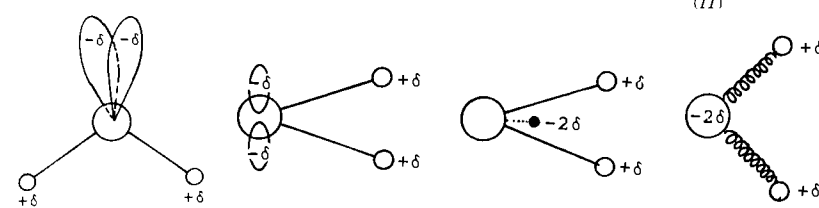
Various types of pair-potential functions for water-water interactions have been proposed so far; they are summarized in Table I.

Potential functions based on the sp^3 -hybrid tetrahedral structure model of water molecules in which two positive and two negative charges are placed at the tetrahedral positions in the molecule have been proposed by Bjerrum (1), Ben-Naim and Stillinger (BNS model) (2), and Stillinger-Rahman (ST2) (3).

An empirical but non- sp^3 -hybrid model has been used by Rowlinson (4), in which electrons in the p_z orbital give rise to negatively charged centers in the molecule.

Pair-potential functions between water molecules estimated by *ab initio* calculations of water dimers have been proposed by Matsuoka,

TABLE I
STRUCTURE MODELS OF THE WATER MOLECULE

Structure type:	Tetrahedral		Nontetrahedral	
	Empirical		Nonempirical	
Flexibility of molecule:	Rigid		Flexible	
Electronic structure:	sp^3 hybrid	$s-p$ nonhybrid	<i>Ab Initio</i> MO	
Author	Bjerrum (1) Ben-Naim-Stillinger (BNS) (2) Stillinger-Rahman (ST2) (3)	Rowlinson (4)	Matsuoka-Clementi-Yoshimine (MCY) (5) Caravetta-Clementi (CC) (6)	Watts (7) Lemberg-Stillinger (8) Rahman-Stillinger-Lemberg (RSL) (9) Stillinger-Rahman (RSL2) (10) Bopp-Jancó-Heinzinger (BJH) (11)
Model				

Clementi, and Yoshimine (MCY) (5) and the functions have been improved by Carravetta and Clementi (CC) (6).

In contrast to molecular models in which the O–H bond length and H–O–H bond angle are fixed, flexible structure models of water molecules have been proposed by Watts (7) and Lemberg and Stillinger (8). The latter have been modified by Rahman, Stillinger, and Lemberg (RSL) (9); Stillinger and Rahman (RSL2) (10); and Bopp, Jancó, and Heinzinger (BJH) (11).

In 1982 Morse and Rice (12) tested different potential functions for water–water interactions that had been proposed and they showed that ST2, MCY, and RSL2 are considered to be the best of their respective groups of models. Potential functions proposed after 1982 with various modifications are equally good in describing water–water interactions. However, the more complicated the potential functions are made by introducing modification, the longer will be the computer time for MD simulations.

B. ION–WATER INTERACTIONS

When we use one of the pair-potential functions to describe ion–water interactions in an electrolyte solution, the polarization of water molecules must be taken into consideration. However, the molecular models for water described previously do not include changes in the charge distribution in the water molecule due to polarization. Kistenmacher, Popkie, and Clementi (KPC) (13) proposed ion–water pair potentials for some alkali metal and halide ions from *ab initio* calculations in which the charge distribution in a water molecule changes with ions, but is independent of the orientation of a water molecule toward an ion, and the distance between the ion and the water molecule. If we use the KPC model together with the MCY model (or any other model of the water molecule) for an aqueous solution of an alkali halide, a water molecule has two different charge distributions at the same time. That is, a water molecule has an MCY-type charge distribution from water–water interactions and a KPC-type charge distribution from ion–water interactions. This contradiction has not been fully solved in the MD simulations of aqueous electrolyte solutions.

The problem of polarization of solvent molecules, as well as solutes in a solution, is a serious one when MD simulations are applied to electrolyte solutions. Attempts have been made to combine *ab initio* calculations with the usual MD simulation process in which the polarization of water molecules caused by ion–water interactions is estimated at each step of the MD calculations, and thus, we can expect that

an elaborate program will soon be proposed in which the polarization effect of ions on water molecules is satisfactorily included.

C. ION-ION INTERACTIONS

Analytical equations used to describe ion-ion interactions can be classified into three categories. In the simplest case an ion is modeled as a Lennard-Jones (LJ) sphere with an elementary charge at the center, where LJ parameters are taken from the isoelectronic noble gases (14). The Born-Mayer-Huggins-type potential is another one of the functions for describing ion-ion interactions, in which the repulsive r^{-12} term of the LJ potential is replaced by an exponential term and an attractive r^{-8} term is added (15). Both are empirically derived and the former gives slightly weaker ion-ion interactions when we adopt the values given in the literature. Ion-ion pair potentials can also be derived from *ab initio* calculations (16).

D. BOUNDARY CONDITIONS

Two different boundary conditions are usually used for simulation processes. One is an isolated system and the other is a bulk system in which a periodical boundary condition is employed. The Ewald summation (17) is often introduced in the calculation of Coulombic interactions. For liquids and solutions the latter system has been used mostly, but the former has been examined in studying the dynamic behavior of a single molecule interacting with a limited number of particles.

1. Isolated Systems

In the course of the analysis of dissolution processes of alkali halide crystals, a piece of a single crystal is dissolved in a limited number of water molecules, and thus, the water molecules and the piece of crystal are placed in an isolated box (Fig. 1).

2. Systems with Periodical Boundary Conditions

Periodical boundary conditions that have widely been examined by MD simulations of liquids and solutions have been employed for simulating the nucleation process of some alkali halides.

The initial state of the systems has been constructed by randomly placing ions and water molecules in numbered small boxes in the basic cell for the bulk system, and by generating random numbers with the aid of a computer. The ions are first fixed and water molecules are then allowed to move freely until a thermal equilibrium has been attained.

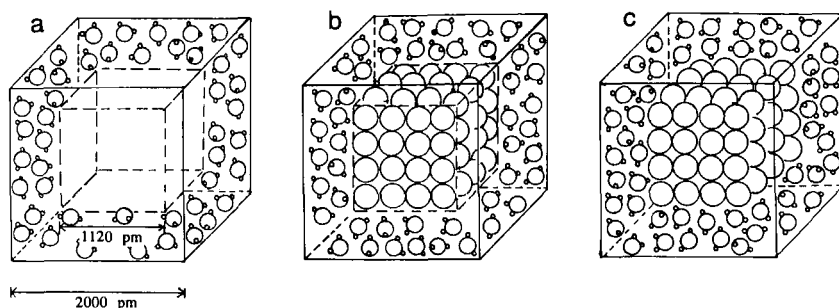


FIG. 1. Simulation procedure before starting the dissolution of a crystal in water: (a) water in the box; (b) water molecules and a crystal in which ions are strongly bound and water molecules are equilibrated with the crystal; (c) the potential function between ions in the crystal is replaced by the function employed in the simulation. The dissolution of the crystal then starts.

In one case all ions and water molecules have been allowed to move freely in the preequilibrium step, but attractions between cations and anions have been assumed to be so weak that the ions have not coaggregated at this stage. This case needs more computer time than the others.

E. PROCEDURE OF THE MD SIMULATIONS

1. Dissolution Process

In this process 512 water molecules and 32 cations and 32 anions have been used. A cubic crystal with the $\{100\}$ faces is placed in a box with a side length of about 2000 pm. Alkali halides examined are LiCl, NaF, NaCl, KF, KCl, and CsF (18–20).

In order to test the effect of the shape of crystals, a sodium chloride crystal with (111) and $(-1-1-1)$ faces, together with $\{100\}$ faces, has been examined. In the crystal 28 cations and 28 anions are included, and the (111) face consists of only sodium ions, and the $(-1-1-1)$ face of chloride ions. No significant difference has in fact been found in the dissolution mechanism of crystals with different faces.

2. Nucleation Process

The nucleation of crystals from supersaturated solutions has been simulated in the NaCl and CsF systems (21). Concentrations of the salts are (i) 9.25 and (ii) 15.42 mol (kg H_2O)⁻¹ for NaCl and (iii) 36.34 mol (kg H_2O)⁻¹ for CsF, which correspond to the systems containing cation (M^+): anion (X^-): water molecule (W) ratios (i) 56:56:336, (ii)

80:80:288, and (iii) 127:127:194. Solubilities of NaCl and CsF are 6.16 and 24.13 mol (kg H₂O)⁻¹, respectively, at 25°C.

F. POTENTIAL FUNCTIONS

In all the simulation processes for dissolution and nucleation, the MCY (5), KPC (13), and Fumi-Tosi (15) potentials have been used for water–water, ion–water, and ion–ion interactions, respectively. The time step Δt has been set at 1.0 fs. The formulae are as follows.

1. MCY Potential

$$\Phi_{\text{water-water}} = q^2 \left\{ \sum (1/r_{\text{H-H}}) - 2 \sum (1/r_{\text{H-M}}) \right\} + 4q/r_{\text{M-M}} + \sum a_{\alpha} \exp(-b_{\alpha} r_{ij}), \quad (1)$$

where M denotes the charge at the negative center of the MCY model, i and j are either H or O atoms; $q = z_{\text{H}}/e = -z_{\text{M}}/2e$, and a_{α} and b_{α} are characteristic constants (Fig. 2).

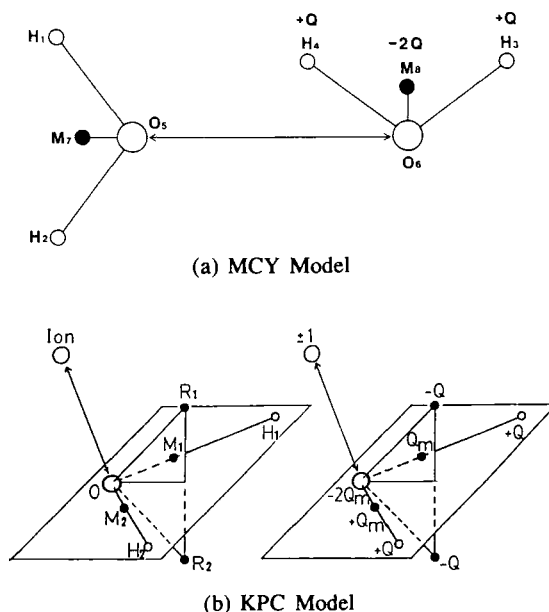


FIG. 2. Models for (a) water–water and (b) ion–water interactions. In (a) the MCY model is used. H₁–H₄, positively charged protons; O₅, O₆, oxygen atoms without charge at the center; M₇, M₈, negatively charged points. In (b) the KPC model is used. Left: positions of atoms and charges; right: amount of charge. H₁, H₂, hydrogen atoms; O, oxygen atom; M₁, M₂, positively charged points; R₁, R₂, negatively charged points.

2. KPC Potential

$$\Phi_{\text{ion-water}} = z_i \sum \{q'/r_{ij}' - q''/r_{ij}''\} + \sum a_k \exp(-b_k r_{uv}), \quad (2)$$

where $q' = z_H/e = -z_R/e$, $q'' = z_M/e = -z_O/e$, and r_{uv} is the distance between atoms u and v in the KPC model (Fig. 2b).

3. Fumi-Tosi Potential

$$\Phi_{\text{ion-ion}} = z_i z_j e^2 / r_{ij} + A_{ij} b_{ij} \exp\{(\sigma_i + \sigma_j - r)/\rho\} - c_{ij}/r^6 - d_{ij}/r^8. \quad (3)$$

Variables z_i and z_j are charges of ions i and j ; A_{ij} is the Pauling factor defined as $A_{ij} = (1 + z_i/n_i + z_j/n_j)$, where n_i and n_j represent the numbers of electrons in the outermost shell of ions i and j , respectively; $c_{ij} = (3/2)\{\alpha_i \alpha_j E_i E_j / (E_i + E_j)\}$ and $d_{ij} = (9/4e^2)c_{ij}(\alpha_i E_i / N_i + \alpha_j E_j / N_j)$, where α denotes the polarizability of ions, N is the number of the total electrons of an ion, and E is the first ionization potential, evaluated from the Equation $E_i^2 = N_i e^2 h^2 / 4\pi^2 m \alpha_i$ for ion i , where h and m are the Planck constant and the mass of the ion, respectively. Values of ρ , b , and σ are estimated from isothermal compressibilities and thermal expansion coefficients of 17 rock-salt-type crystals of alkali halides by Fumi and Tosi (15).

G. PAIR CORRELATION FUNCTION AND RUNNING COORDINATION NUMBER

The correlation function $g_{ij}(r)$ for the i - j atom pair is defined as

$$g_{ij}(r) = \frac{1}{4\pi\rho_i r^2 \Delta r} \cdot \frac{N_{ij}(r)}{N_i}, \quad (4)$$

where $N_{ij}(r)$ represents the numbers of j particles in the range r to $r + \Delta r$ around the central ion i , and N_i is the total number of i particles in a given volume V . The parameter ρ_i is the number density.

The number of j particles around a particle i is given as a function of the distance r of the j particles from the particle i and is defined as the running coordination number $n_{ij}(r)$:

$$n_{ij}(r) = 4\pi\rho_i \int_0^r r^2 g_{ij}(r) dr. \quad (5)$$

III. The Solution X-Ray Diffraction Method

The solution X-ray diffraction method has been widely used for the structural analysis of liquids, solvated ions, and complexes in solution,

and excellent reviews have been published on these subjects (22–25). This method has been employed to determine the average size of ionic clusters of alkali halides in their nearly saturated or supersaturated aqueous solutions in order to compare results obtained from the MD simulations with experimental results.

The structures of liquids and solutions are determined by analyzing the radial distribution functions $D(r)$ or $G(r) = D(r)/4\pi r^2 \rho_0$, where $D(r)$ is given by measuring the intensities of the scattered monochromatized X-ray beams at different angles (the angle dispersive method) or scattered white X-rays at a given angle (the energy dispersive method). The latter method is unfavorable for systems containing relatively heavy atoms from which fluorescence X-rays are usually emitted upon irradiation. In the former method, the fluorescence X-rays can be cut by placement of a monochromator between a sample solution and the detector. A schematic of the apparatus used for measurements with a monochromatized X-ray beam is shown in Fig. 3.

A. FUNCTIONS USED FOR THE DIFFRACTION STUDIES

The radial distribution function $D(r)$ is given by

$$D(r) = 4\pi r^2 \rho_0 + \frac{2r}{\pi} \int_0^{s_{\max}} s \cdot i(s) \cdot M(s) \cdot \sin(rs) ds, \quad (6)$$

where r denotes an interatomic distance, ρ_0 the average electron density, and s_{\max} the maximum s value attained in the experiment; $s = 4\pi\lambda^{-1} \sin \theta$, λ wavelength of the X-ray used, and 2θ is the scattering angle.

The reduced intensities $i(s)$ are calculated with respect to a given stoichiometric volume of the solution according to

$$i(s) = KI(s) - \sum n_j f_j(s)^2, \quad (7)$$

where $I(s)$ is the corrected experimental intensity, K is the normalizing factor to convert $I(s)$ values to the absolute scale, n_j is the number of atoms j in the stoichiometric volume, and $f_j(s)$ is the scattering factor of atom j at s corrected for the anomalous dispersion. The term $M(s)$ denotes the modification function and is of the form

$$M(s) = \left\{ \frac{\sum [n_j f_j(0)]^2}{\sum [n_j f_j(s)]^2} \right\} \cdot \exp(-ks^2), \quad (8)$$

where the damping factor $k = 0.01 \text{ pm}^2$ has been used throughout. The structure function $s \cdot i(s)$ is described in terms of the intramolecular and

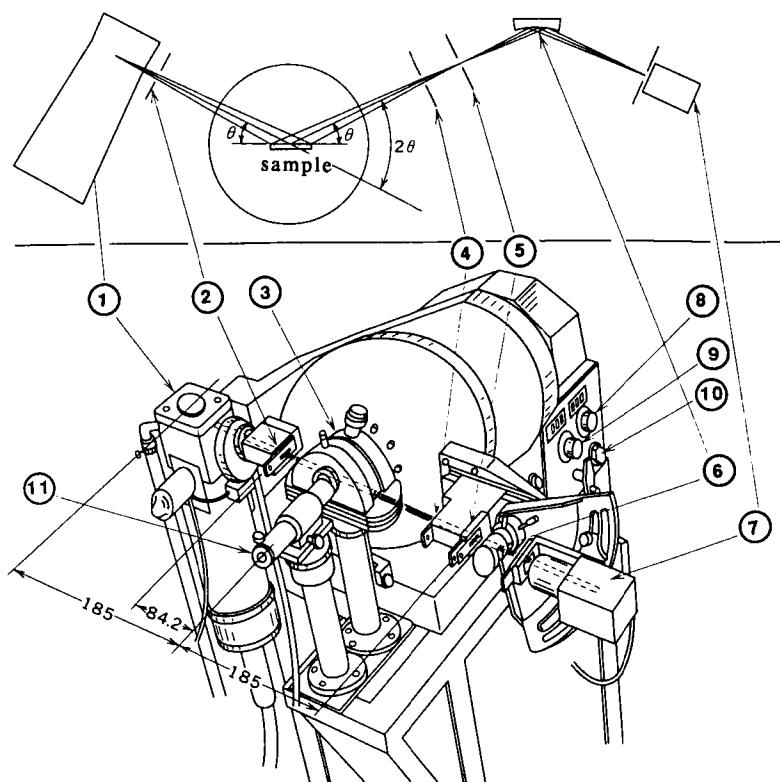


FIG. 3. A schematic of an X-ray diffractometer. 1, X-ray source; 2, divergent slit; 3, sample cover with beryllium window; 4, scattering slit; 5, receiving slit; 6, monochromator; 7, scintillation counter; 8, knob for adjusting the angle of the counter; 9, knob for adjusting the angle of the X-ray tube; 10, knob for changing the angle step; 11, telescope for observing the sample height. Numerals in the figure indicate the length between the relevant parts.

intermolecular interactions as

$$s \cdot i(s) = s \sum n_{pq} c_{pq}(s) j_0(sr_{pq}) \exp(-b_{pq}s^2) - 4\pi\rho_0 \sum n_p n_q c_{pq}(s) R_{pq}^2 j_1(sR_{pq}) \exp(-B_{pq}s^2), \quad (9)$$

where $c_{pq} = f_p(s)f_q(s)M(s)$ and r_{pq} , b_{pq} , and n_{pq} denote the distance, temperature factor, and frequency factor of the p-q atom pair, respectively. The temperature factor b is related to the mean square variation of the distance l by the equation $b = l^2/2$. The frequency factor n_{pq} corresponds to the coordination number usually defined in coordination chemistry. The term R_{pq} is the distance beyond which a continuous

distribution of atoms of type q around the p -type atom in the center is assumed, and B_{pq} is the parameter describing the sharpness of the boundary at R_{pq} . The term $j_m(x)$ represents the spherical Bessel function of the m th order.

The structure parameters r_{pq} , b_{pq} , and n_{pq} in Eq. (9) are finally refined by the least-squares method to minimize the error square sum U ,

$$U = \sum_{s_{\min}}^{s_{\max}} w \{i_{\text{calc}}(s) - i(s)\}^2 \quad (10)$$

and $w = s^2$ has been used in all the least-squares calculations.

B. PROCEDURES OF THE X-RAY DIFFRACTION EXPERIMENTS

X-Ray diffraction experiments have been carried out for four saturated and supersaturated aqueous solutions of simple salts (26), in order to compare the results obtained by the MD simulations (21) with the experimental results. The aqueous solutions examined were 6.18 mol (kg H₂O)⁻¹ NaCl (H₂O/salt molar ratio, 8.98), 4.56 mol (kg H₂O)⁻¹ KCl (molar ratio, 12.18), 16.15 mol (kg H₂O)⁻¹ KF (molar ratio, 3.44), and 31.96 mol (kg H₂O)⁻¹ CsF (molar ratio, 1.74) (26). The saturation concentrations of these salts at 298 K were 6.15 mol (kg H₂O)⁻¹ for NaCl, 4.81 mol (kg H₂O)⁻¹ for KCl, 17.50 mol (kg H₂O)⁻¹ for KF, and 24.13 mol (kg H₂O)⁻¹ for CsF. The supersaturated solutions were stable for several weeks without formation of crystals.

IV. The Dissolution Process of Rock-Salt-Type Alkali Halide Crystals

Since ion-ion-pair potentials have been thoroughly investigated for rock-salt-type crystals by Tosi and Fumi (15) and those for other type salts have not been as well studied, the MD simulations have been carried out for alkali fluoride and chloride crystals of the rock-salt type: NaF, KF, CsF, LiCl, NaCl, and KCl. Due to the limitation of computer times, the simulations have been carried out for only 12 to 20 ps depending on the systems. The experimental conditions for the simulations are summarized in Table II.

Water molecules are assumed to be completely elastic with respect to their center of gravity on collision to the rigid wall. Ions can pass through the wall, and thus we have introduced a switching function $S_w(x)$ to cut off electrostatic effects arising from ions that have gone

TABLE II

EXPERIMENTAL CONDITIONS OF MD SIMULATIONS FOR DISSOLUTION OF ALKALI FLUORIDE AND CHLORIDE CRYSTALS AT 25°C^a

	NaF	KF	CsF	LiCl	NaCl	KCl
l (pm)	1,938	1,975	2,019	1,963	1,993	2,039
t (ps)	12.0	20.0	12.0	12.0	20.0	20.0
N	12,000	20,000	12,000	12,000	20,000	20,000

^a Numbers of cations, anions, and water molecules in the systems are 32, 32, and 216, respectively. l , side length of the box; t , total time for the simulation; N , number of steps. Time step: 10^{-15} s.

beyond the wall. The switching function used is

$$\begin{aligned} S_w(x) &= 1 & \text{for } -l/2 \leq x \leq l/2 \\ S_w(x) &= \exp \{-\alpha_i(|x| - l/2)^2\} & \text{for } |x| > l/2, \end{aligned} \quad (11)$$

where x is any one of the three Cartesian coordinates, their origin being the middle of the box. The parameter α_i has been defined as $1/(0.3954r_i)^2$, where r_i denotes the ionic radius of i . Values for r_i and α_i are listed in Table III.

Typical results for the evolution of the distances R of ions from the center of the box and corresponding snapshots of the dissolution process are shown in Fig. 4. Water molecules are omitted in this figure. The dissolution process of NaCl and CsF crystals has been recorded on video tape (27), in which the movement of water molecules is included. From these the rotational, librational, and translational motions of water molecules are observed. The video pictures show the behavior of water molecules around the "structure breaking" chloride ions, and the slower motion of water molecules around the "structure making" fluoride as opposed to chloride can be seen. Color photographs of the snapshots for the dissolution of an NaCl crystal, together with water molecules, within 7 ps are shown in Fig. 5.

TABLE III

RADII OF IONS AND α VALUES OF THE SWITCHING FUNCTION $S_w(x)$

	Li ⁺	Na ⁺	K ⁺	Cs ⁺	F ⁻	Cl ⁻
r_i (pm)	74	102	138	170	133	181
α_i (10^{-4} pm ⁻²)	11.68	6.148	3.359	2.213	3.616	1.952

A. ALKALI FLUORIDES

1. *NaF*

No dissolution of ions has been observed within 12 ps, although the structure of the crystal becomes distorted due to thermal vibrations of the lattice. The fluctuation of positions of ions is more pronounced for F⁻ than for Na⁺ (Fig. 4a).

2. *KF*

No dissolution has been observed within 20 ps. The distortion of lattice of the crystal is less pronounced than that of NaF despite the smaller lattice energy of KF than NaF, probably due to the smaller hydration energy of K⁺ than Na⁺.

3. *CsF*

Three fluoride ions have dissolved within 12 ps. Some fluoride ions move around the surface of the crystal but are not separated from it. The position of fluoride in the crystal fluctuates more rapidly than that of cesium (Fig. 4b). The mechanism of dissolution of the CsF in water will be discussed in a later section.

B. ALKALI CHLORIDES

1. *LiCl*

Eight chloride ions have dissolved but no dissolution of cations has been observed within 12 ps. Thus, 12 ps after the start of dissolution the crystal has a composition [Li₃₂Cl₂₄]⁸⁺. Four chloride ions at the corners of the crystal divide at the very beginning of the process. The dissolution process then stops for a few picoseconds, after which some chloride ions dissolve from the corner-like positions of the distorted crystal. Finally, a further dissolution of chloride ions is observed for 10 ps. The fluctuation of positions of ions in the crystal is more enhanced for Cl⁻ than for Li⁺.

2. *NaCl*

Five chloride ions have dissolved within 7 ps and no further dissolution of ions is observed within 20 ps. Thus a microcluster having a composition [Na₃₂Cl₂₇]⁵⁺ remains in the water for more than 15 ps. No prediction is possible as to when the sodium ions start to dissolve. The displacement of Na⁺ and Cl⁻ ions are depicted in Fig. 4c, and color photographs depicting the situation after are shown in Fig 5.

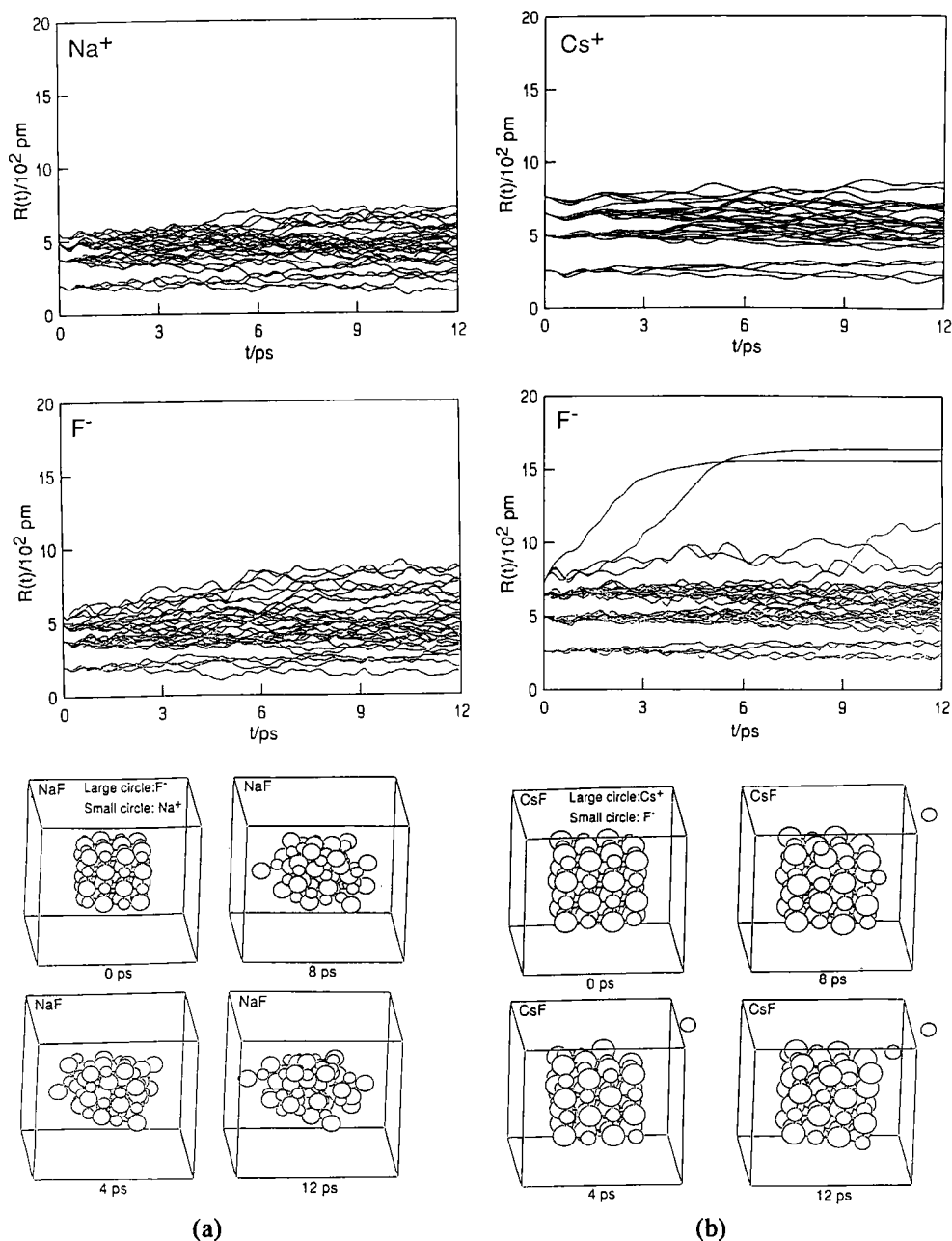


FIG. 4. Evolution of the distance R from the center of a box of ions of alkali halide crystals in water, and corresponding diagrams for (a) NaF, (b) CsF, (c) NaCl, (d) CsF with the Cs atom having the same atomic weight as the F atom.

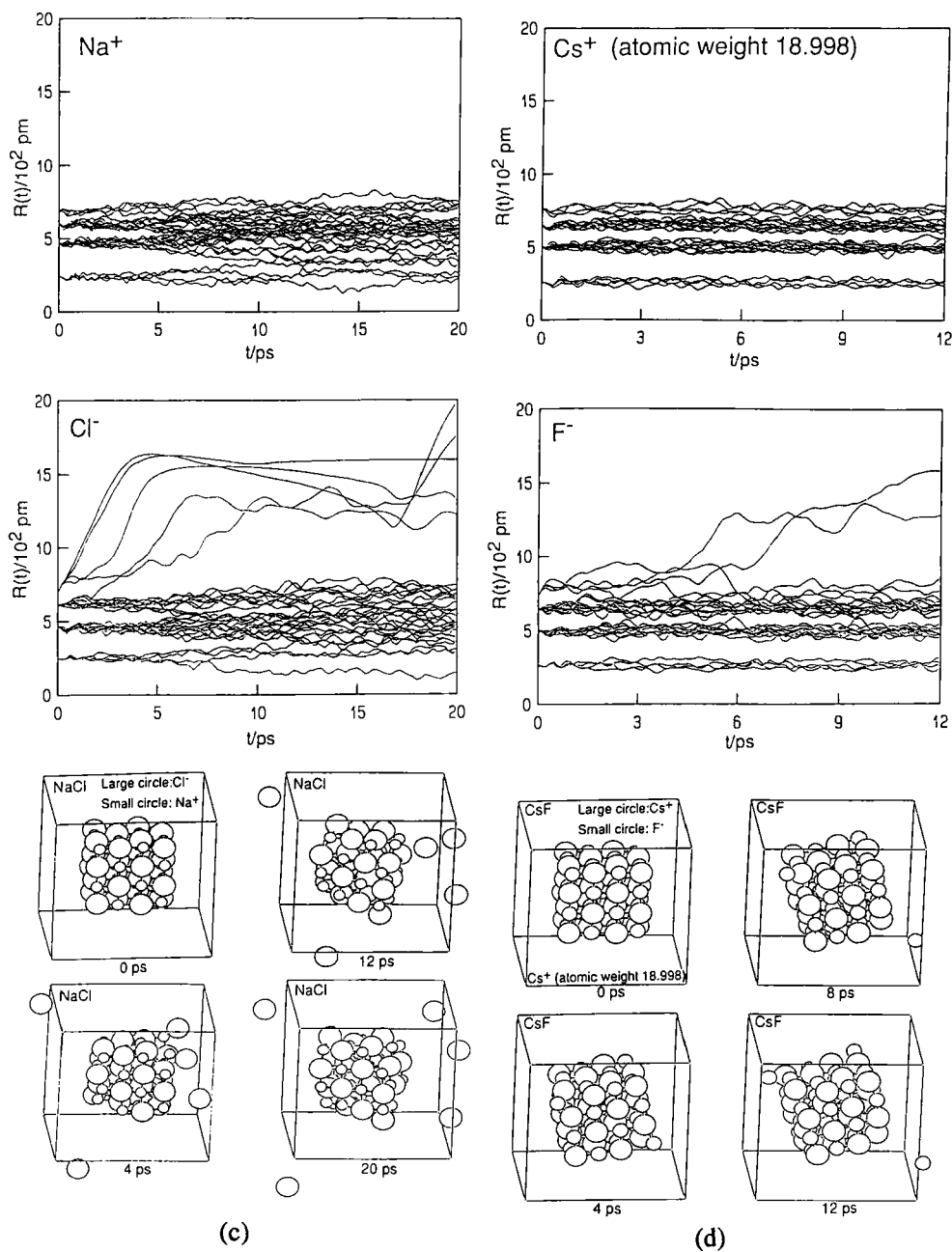


FIG. 4. (Continued)

3. *KCl*

No dissolution of ions has been observed within 20 ps. The distortion of the crystal structure of KCl is greater than that of KF due to the smaller lattice energy of the former.

Results obtained from studies on alkali fluoride and chloride crystals show that alkali metal ions (cesium in this case) dissolve first in the former, whereas chloride ions dissolve first in the latter. The differences are accounted for by the ionic sizes of the cation and anion, which are significantly different in the two cases. The dissolution of the second ion occurs soon afterward, although we cannot predict when. If the size of the cation and anion is about the same, the dissolution process is retarded.

C. EFFECTS OF MASSES AND THE CRYSTAL FACES

1. *Mass Effect*

The mass effect of ions on the dissolution mechanism has been tested by using Cs^+ ions with the same atomic weight as that of F^- (atomic weight: 18.998). The frequencies of thermal vibrations of Cs^+ and F^- are almost the same and although no dissolution of Cs^+ ions has been observed, two fluoride ions have dissolved (Fig. 4d).

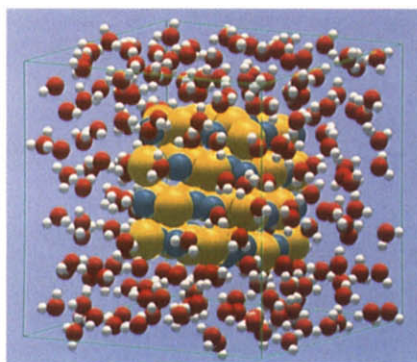
2. *The Effect of Crystal Faces*

The effect of crystal faces on the dissolution has been investigated using a NaCl crystal with (111) and (-1-1-1) faces together with {100} faces to compare results with studies for crystals having only {100} faces. Although fewer chloride and no sodium ions dissolve within 12 ps, essentially no difference is observed for the dissolution of NaCl crystals with different faces.

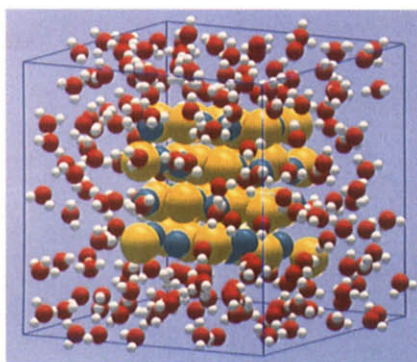
The deformation of crystal seems to be more enhanced in the corner-cut crystal than in the cubic one within the same dissolution period.

D. DISSOLUTION MECHANISMS

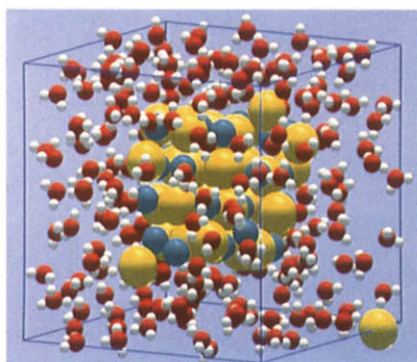
It has been observed that an ion at the corner of a crystal divides first. Forces acting on the ion can be divided into three components: (i) forces from the rest of the co-ions, (ii) forces from all counter ions, (iii) forces from all water molecules. The sign of the forces is defined as positive when directed away from the center of the box. Figure 6 shows the evolution of these forces on a cation at one corner and an anion at the opposite corner for the system NaF in which no ions have dissolved,



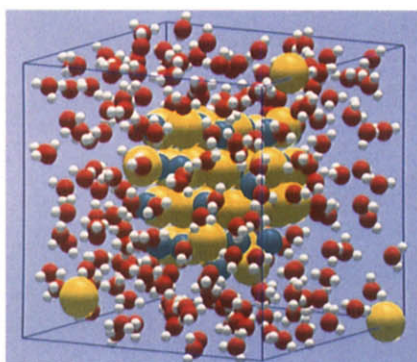
Time = 0.00 ps



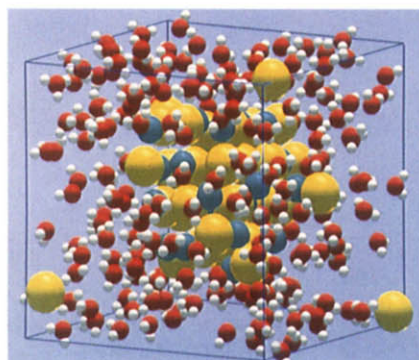
Time = 1.00 ps



Time = 3.00 ps



Time = 5.00 ps



Time = 7.00 ps

FIG. 5. Photographs of the dissolution process of NaCl crystals with the {100} faces from 0 to 7 ps.

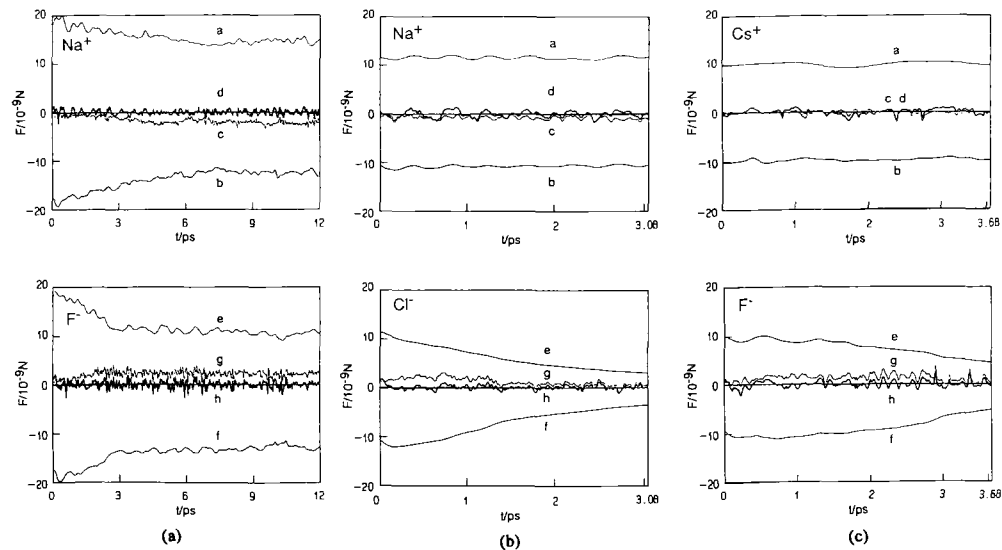


FIG. 6. Evolution of the average forces acting on a cation at a corner, and the anion at the opposite corner of (a) NaF, (b) NaCl, (c) CsF crystals. Curves a and e: forces resulting from all co-ions; curves b and f: forces from all counter-ions; curves c and g: forces resulting from all water molecules; curves d and h: The sum of the forces $a + b + c$ and $e + f + g$, respectively. Forces are positive when pointing away from the center of the box.

and of CsF and NaCl where in both cases some anions have dissolved. Curves a and e show forces (i), curves b and f forces (ii), and curves c and g forces (iii). Curves d and h, drawn as thick lines, represent the sum of forces (i), (ii), and (iii).

The sum of the three forces fluctuate around zero, indicating that the ions remained close to their equilibrium positions. The interionic forces (a, b, e, and f) decrease with time when the crystal is deformed or if ions leave it.

With regard to the ion–water interactions, one can see that the water molecules exert a small force on the cations toward the liquid (KF), or practically no force (CsF, KCl), but in the most cases (NaF, LiCl, NaCl) a force toward the crystal. In all cases no cation has dissolved within the time examined. On the other hand, water molecules exert a force on the anions toward the liquid in all cases. If the force is large (CsF, LiCl, NaCl) the anions dissolve; if it is small (KF, KCl) the anions do not dissolve. An exception is NaF, where the force acting on fluoride at a corner is large but no fluoride dissolves. In this case, however, the crystal structure of the NaF deforms quite remarkably, and the whole crystal seems to be in a “semidissolved” state (Fig. 4a).

From these observations we may explain the dissolution mechanism of ions from crystals as follows. A corner ion with three counter-ions as neighbors in a rock-salt-type crystal interacts with water molecules and the neighboring counter-ions by bridging them. If the corner ion is an anion, the ion attracts one of the $\delta+$ charged protons in a water molecule to form a hydrogen bond to make the anion \cdots H–O bond linear, while a $2\delta-$ charged oxygen atom in the water molecule interacts with a neighboring cation, and thus, a repulsive force arises between the proton ($\delta+$) and the cation (M^+) or between the oxygen atom ($2\delta-$) and the anion (X^-). If the cation–water interaction is stronger than the anion–water interaction, the anion is squeezed out and liberated from the crystal surface. When the anion–water interaction is stronger, the anion leaves the crystal in the company of the water molecule. In fact, such phenomena have been seen on video. If the corner ion is a cation that is larger than the counter-anion, as in the case of CsF, the repulsive forces between the anion and the oxygen atom in the water molecule hydrated to the anion may not be strong enough to liberate the large cation, because the repulsive force between M^+ and $H^{\delta+}$ is partly compensated by the attractive force between M^+ and $O^{2\delta-}$. In most cases anions are larger than the cations. An exception is the case for LiF, which is sparingly soluble in water.

Thus, the asymmetric charge distribution among an oxygen and two

hydrogen atoms in a water molecule may play an essential role in the dissolution process of ions from crystal surfaces.

V. Nucleation Processes of Alkali Halide Crystals

a. Ion-Pair Formation in Solutions under Saturation. A number of studies have been carried out on the formation of ion pairs with various combinations of cations and anions in aqueous solution by the conductometric method. However, in aqueous alkali halide solution the ion-pair formation rarely occurs, because of the relatively strong hydration of the ions and rather weak cation–anion interactions.

In aqueous solutions of low concentration, when theories of ionic conductivities are applicable, no ion pairs will be formed in the case of the lithium and sodium halides at room temperature. Even in 13.9 mol (kg H₂O)^{−1} LiCl aqueous solution where the molar ratio of LiCl to H₂O is 1:4, essentially no ion pairs between Li⁺ and Cl[−] ions are formed around 25°C, according to an MD simulation (28). Formation of the 1:1 ion pair between Li⁺ and Cl[−] in aqueous solution is, however, concluded in 18.5 mol (kg H₂O)^{−1} aqueous solution where the $n_{\text{LiCl}}:n_{\text{H}_2\text{O}}$ molar ratio is 1:3, which is close to the saturation concentration of LiCl in water (29). Formation of the 1:1 Li⁺·Cl[−] ion pair has been suggested by a neutron diffraction method (30), but the data derived from such measurements were not in good agreement with the simulation results. No evidence has been found for ion-pair formation between Li⁺ and I[−] ions at 20 and 50°C in 2.78 and 6.05 mol (kg H₂O)^{−1} aqueous lithium iodide using the solution X-ray diffraction method (31).

In almost saturated aqueous solutions of NaCl [6.18 mol (kg H₂O)^{−1}] and KCl [4.56 mol (kg H₂O)^{−1}], about 30 and 60 mol%, respectively, of the ions form contact ion pairs according to X-ray diffraction measurements (26). The Na⁺–Cl[−] and K⁺–Cl[−] bond lengths have been evaluated to be 282 and 315 pm. The ion pairs, as well as free ions, are certainly hydrated, and the average hydration numbers of the Na⁺ and Cl[−] ions in the NaCl solution are 4.6 and 5.3, respectively, and those of K⁺ and Cl[−] ions in the KCl solution are both 5.8. No diffraction measurement has been carried out yet, however.

Potassium fluoride has a higher solubility than NaCl and KCl in water. An MD simulation has been examined for 16.15 mol (kg H₂O)^{−1} KF aqueous solution at about 25°C [the concentration of a saturated solution is 17.50 mol (kg H₂O)^{−1} at 25°C] and reveals the formation of ionic clusters that contain more than 1:1 ion pairs. The average

coordination number of the K^+-F^- pairs has been found to be 2.29 (26). The K^+-F^- interatomic distance in the clusters has been determined to be 269 pm, and the interatomic distances and the average coordination numbers are 388 pm and 1.94 respectively for K^+-K^+ pairs, and 432 pm and 1.6 respectively for $\text{F}^- - \text{F}^-$ pairs. The latter pair has a larger interatomic distance than the former despite the smaller ionic size of the F^- than K^+ .

Ion-pair formation is more clearly seen in cesium halide solutions than in other alkali halide solutions discussed previously, because of weak hydration of cesium ions. The formation of contact ion pairs between Cs^+ and F^- ions has been suggested by Szász and Heinzinger (33) in 2.2 mol dm^{-3} aqueous solution.

According to the MD simulations examined for cesium iodide solutions of 2.78 mol dm^{-3} ($\text{CsI}:\text{H}_2\text{O} = 1:20$) at 25 and 64°C and 5.56 mol dm^{-3} ($\text{CsI}:\text{H}_2\text{O} = 1:10$) at 64°C (34), higher ion pairs than 1:1 form in the 2.78 mol dm^{-3} solution, but formation is suppressed as the temperature is raised. Thus, ion-pair formation reactions between cesium and iodide, both of which are weakly hydrated, must be exothermic, although no thermodynamic data are available in the literature. The increase in concentration at a given temperature (64°C) enhances the formation of the ionic aggregates from $n_{\text{CsI}} = 1.07$ to 1.80.

An X-ray diffraction study supports the result of the MD simulations (31). The Cs–I bond distance has been experimentally determined to be 388 and 385 pm at 20 and 50°C, respectively. The coordination number of the Cs–I pairs has been evaluated to be 0.8 in the 2.78 mol $(\text{kg H}_2\text{O})^{-1}$ solution at 20 and 50°C, which increases to 1.18 in the 5.56 mol $(\text{kg H}_2\text{O})^{-1}$ solution at 50°C. The results of the X-ray diffraction measurements agree fairly well with those obtained by MD simulations carried out under similar conditions (34).

b. Formation of Highly Aggregated Species of Alkali and Halide Ions in Supersaturated Solutions. Supersaturated solutions are usually unstable, but in some cases can be kept for more than a week without deposition of crystals. Cesium iodide is a good example, and it is possible to prepare a 31.96 mol $(\text{kg H}_2\text{O})^{-1}$ aqueous solution at 25°C, which is oversaturated by 132.4%. The molar ratio between the salt and water is 1:1.74. The solution can be used for X-ray diffraction measurements to study the solution structure, and the results show that highly aggregated species are formed in solution (31). Since the coordination numbers of the pairs Cs^+-F^- (n_{CsF}), Cs^+-Cs^+ (n_{CsCs}), and $\text{F}^- - \text{F}^-$ (n_{FF}) are 3.33, 2.35, and 5.3, respectively, the coordination of ions around a central ion may occur beyond the first coordination shell of the central

ion. The different coordination numbers of n_{CsCs} and n_{FF} , where the differences are larger than the uncertainties in the simulation calculations, suggest that the number of cations and anions in the cluster may not be the same, and that the clusters are charged. The n_{FF} value contains a much larger uncertainty than n_{CsCs} , however. The contact distance Cs^+-F^- has been evaluated as 312 pm, and the Cs^+-Cs^+ and F^--F^- nonbonding distances are determined as 442 and 548 pm, respectively, which are close to $\sqrt{2}$ and $\sqrt{3}$ times the Cs^+-F^- distance, respectively.

c. MD Simulations for the Nucleation Process of Alkali Halide Crystals. The nucleation process of alkali halide crystals has been simulated in supersaturated aqueous solutions of NaCl, 9.25 and 15.42 mol (kg H₂O)⁻¹, and CsF, 36.34 mol (kg H₂O)⁻¹ (35), using the periodic boundary conditions and with application of the Ewald summation (17).

The coagulation of ions in these solutions is as depicted in Fig. 7 (27). Small-size clusters containing a few cations and anions at the beginning of the simulation calculations grow to large clusters with time as expected. The shape of the cluster is irregular, and unequal numbers of cations and anions are present, with the result that the clusters are charged therefore.

The growth of clusters is shown as the change in the running coordination number $n_{ij}(r)$ around a cation M^+ , and an anion X^- as defined by Eq. (5). Values of n_{MX} , n_{MM} , and n_{XX} are summarized in Table IV.

The running coordination numbers $n(r_1)$ and $n(r_2)$ increased with time and reached constant values. The coagulation of ions might still occur in the range of the third coordination sphere or even further with time, although the $n(r_3)$, $n(r_4)$, and so on, have not been calculated. From the diagrams in Fig. 7, however, we see that the increase in the size of the microclusters or nuclei is not remarkable after 12 ps. From the results in Table IV $n_{\text{MM}}(r_2)$ is larger than $n_{\text{XX}}(r_2)$ in all cases, and the number of cations is therefore larger than that of anions in the clusters. The result is the reverse of that found in X-ray diffraction experiments (31), in which a larger number is given for n_{FF} than for n_{CsCs} . However, the former contains a fairly large uncertainty.

Since the degree of supersaturation and concentration of salt are largest in the cesium fluoride system, the largest clusters seem to be formed in solution, as expected. However, since the number of ions in solutions examined are too small, the clusters cannot grow to the size of nuclei of crystals. Nevertheless, it can be seen from Fig. 7 that small aggregates, which may be regarded as embryos for crystallization, become the cores of crystals, and have an irregular shape.

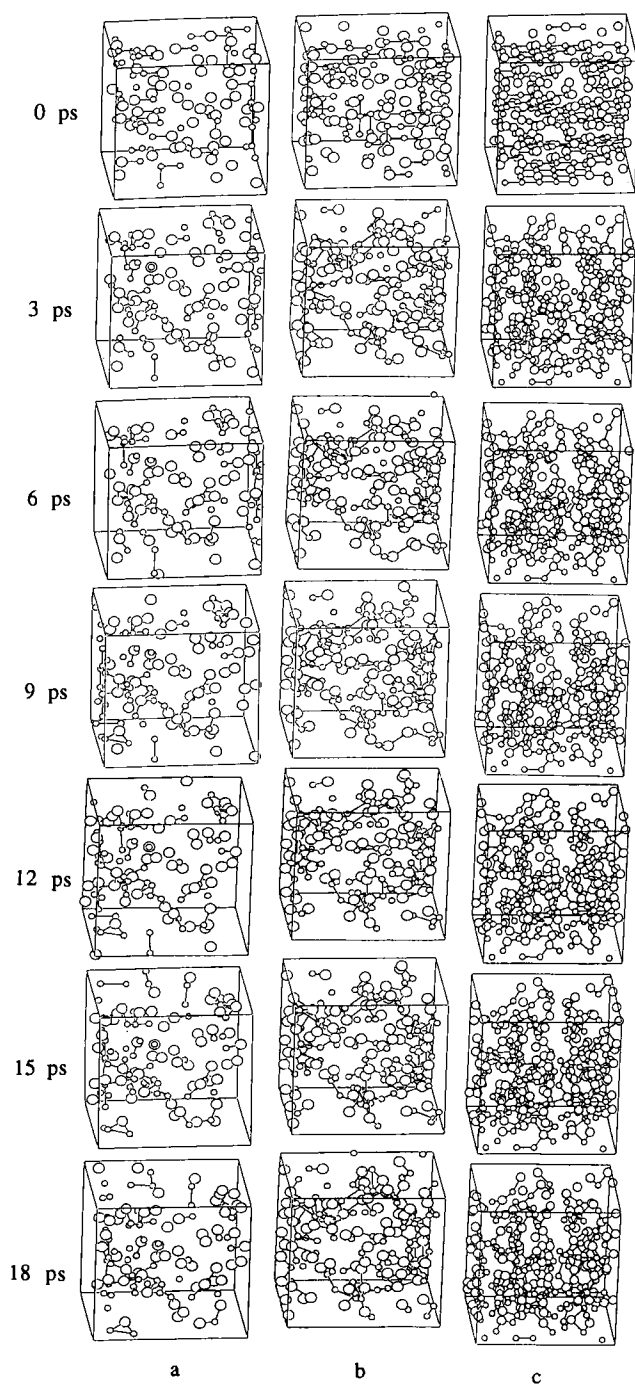


TABLE IV

THE TIME DEPENDENCE OF THE RUNNING COORDINATION
NUMBERS n_{ij} WITHIN THE FIRST AND SECOND
COORDINATION SPHERES^a

	n_{ij}	r (pm)	Time (ps)			
			0	6	12	18
9.25 M NaCl	n_{NaCl}	282.5	0.13	0.64	0.55	0.55
		489.3	1.98	2.36	2.38	2.43
	n_{NaNa}	399.5	0.95	0.69	0.69	0.58
		564.5	3.75	3.02	3.02	2.84
	n_{ClCl}	399.5	0.15	0.18	0.18	0.18
		564.5	2.51	2.15	2.15	2.25
15.42 M NaCl	n_{NaCl}	282.5	0.00	1.25	1.25	1.24
		489.3	3.53	3.55	3.65	3.76
	n_{NaNa}	399.5	0.94	0.96	0.94	0.99
		564.5	4.43	4.41	4.43	4.46
	n_{ClCl}	399.5	0.00	0.71	0.81	0.78
		564.5	4.20	4.15	4.18	4.25
36.34 M CsF	n_{CsF}	301.5	1.66	1.79	2.01	1.90
		522.1	5.15	6.06	6.01	5.85
	n_{CsCs}	426.3	1.65	2.24	2.29	2.27
		602.5	8.17	8.78	9.00	9.30
	n_{FF}	426.3	3.00	2.37	2.37	2.38
		602.5	8.54	8.33	8.54	8.76

^a The term r is the upper limit of the integral in Eq. (5) and the smaller and the larger values indicate the ranges of the first and second coordination spheres, respectively. These are defined in the present work as $r_1 = (1/\sqrt{2})r_L$ and $2r_L$ for ions with different and the same charges, respectively, in the first sphere coordination sphere, and $r_2 = (\sqrt{3}/2)r_L$ and r_L for different the same charges, respectively, in the second coordination sphere. The term r_L denotes the lattice constant, and m stands for mol (kg H₂O)⁻¹.

FIG. 7. ORTEP diagrams of supersaturated (a) 9.25 mol (kg H₂O)⁻¹ NaCl, (b) 15.42 mol (kg H₂O)⁻¹ NaCl (small and large circles indicate Na⁺ and Cl⁻ ions, respectively), and (c) 36.34 mol (kg H₂O)⁻¹ CsF solutions. Large and small circles indicate Cs⁺ and F⁻ ions, respectively.

It may still be difficult to generalize the mechanism of nucleation of crystals in supersaturated solutions because of the lack of statistics, but the results seem to suggest a possible understanding of the nucleation mechanism. In the real case, charged microclusters with irregular forms may be produced at a very early stage of formation, and then gather to form larger aggregates. Subsequently after the size of the aggregate exceeds a limiting size, crystal growth begins and can be observed under a microscope. However, we still do not know whether the irregular shape of the core will be a regular form in the course of crystal growth, or an irregular form will remain at the core of a large crystal.

VI. Molecular Approaches to Crystal Formation and Growth

A huge amount of knowledge has been accumulated about chemistry of crystal formation and growth, mainly from the viewpoint of morphology, crystallography, and phase diagrams. Many theories for explaining crystal formation and growth have been proposed, and observations that support the theories have resulted from the use of microscopes and from X-ray crystallographic analysis as well as the application of other experimental techniques. However, the gap is still fairly large between morphological or crystallographic investigations and molecular approaches to the elucidation of the mechanism of crystal formation and growth. Studies on the structure of solutions containing species that will form crystals may result in an understanding of the mechanism. In the following sections results of case studies that relate to the formation of relatively simple crystals will be considered from the viewpoint of coordination chemistry.

A. WHY DO $\text{CoCl}_2 \cdot 4\text{H}_2\text{O}$ CRYSTALS FORM VERY SLOWLY AND $\text{CoCl}_2 \cdot 2\text{H}_2\text{O}$ CRYSTALS READILY CONVERT TO $\text{CoCl}_2 \cdot 6\text{H}_2\text{O}$ UPON COOLING?

In aqueous chloride solution, cobalt(II) forms octahedral $[\text{Co}(\text{H}_2\text{O})_6]^{2+}$, $[\text{CoCl}(\text{H}_2\text{O})_5]^+$, and $[\text{CoCl}_2(\text{H}_2\text{O})_4]^0$ and tetrahedral $[\text{CoCl}_3(\text{H}_2\text{O})]^-$ and $[\text{CoCl}_4]^{2-}$ complexes (36–42). With an increase in temperature, the formation of higher complexes is enhanced, because the enthalpies of formation of the complexes, ΔH_n^0 ($n = 1-4$), are all positive (43).

Cobalt(II) dichloride di-, tetra-, and hexahydrate crystals form over the temperature range $>58^\circ\text{C}$, $58-49^\circ\text{C}$, and $<49^\circ\text{C}$, respectively. The

temperature range where $\text{CoCl}_2 \cdot 4\text{H}_2\text{O}$ can exist is relatively narrow, and thus $\text{CoCl}_2 \cdot 2\text{H}_2\text{O}$ crystals change to $\text{CoCl}_2 \cdot 6\text{H}_2\text{O}$ upon cooling solutions of dihydrate crystals and vice versa. The formation of $\text{CoCl}_2 \cdot 4\text{H}_2\text{O}$ crystals can hardly be observed at all in cooling and heating processes at a normal rate of say, $1.5^\circ\text{C min}^{-1}$. When solutions are kept for several days at around 58°C , dark red approximately cubo-octahedral crystals of $\text{CoCl}_2 \cdot 4\text{H}_2\text{O}$ form. Crystals of $\text{CoCl}_2 \cdot 2\text{H}_2\text{O}$ are pink, whereas those of $\text{CoCl}_2 \cdot 6\text{H}_2\text{O}$ are a darker pink. From the color, it is obvious that all of the complexes in these crystals have an octahedral structure.

The structures of cobalt(II) complexes in crystals have been determined by X-ray diffraction (44). The results obtained show that cobalt(II) forms the *trans*- $[\text{CoCl}_2(\text{H}_2\text{O})_4]$ and *trans*- $[\text{CoCl}_4(\text{H}_2\text{O})_2]$ moieties in the hexa- and dihydrate crystals, respectively. The former exists as an isolated unit structure, whereas chloride ions in the latter are shared by adjacent $[\text{CoCl}_4(\text{H}_2\text{O})_2]$ units. On the other hand, the two chloride ions of the $[\text{CoCl}_2(\text{H}_2\text{O})_4]$ moiety in the tetrahydrate crystals are located at the *cis*-positions (Fig. 8). The *cis*-*trans* transformation occurs due to hydrogen-bonding intermolecular interactions in the crystals. It is expected that the structural change between *trans*- $[\text{CoCl}_2(\text{H}_2\text{O})_4]$ and *trans*- $[\text{CoCl}_4(\text{H}_2\text{O})_2]$ might occur more readily than that between *trans*- $[\text{CoCl}_2(\text{H}_2\text{O})_4]$ and *cis*- $[\text{CoCl}_2(\text{H}_2\text{O})_4]$, because in the former two water molecules at the *trans*-position must be substituted with two chloride. This may proceed rapidly in solution, and the complexes formed in solution build up into crystals.

In the transformation reaction of $\text{CoCl}_2 \cdot 6\text{H}_2\text{O}$ to $\text{CoCl}_2 \cdot 4\text{H}_2\text{O}$, on the other hand, the unit of composition, $[\text{CoCl}_2(\text{H}_2\text{O})_4]$, remains unchanged, but chloride ions in the former are in the *trans*-position and in the latter, the *cis*-positions. It is expected that $[\text{CoCl}_2(\text{H}_2\text{O})_4]$ in solution is in the *trans*-form, and that the *cis*-structure is generated on formation of the crystal phase assisted by hydrogen bonding between the chloride and water molecules in adjacent units.

The mechanism of the *cis*-*trans* transformation in crystals is not yet clear. In Table V the structures of $\text{MX}_2 \cdot 4\text{H}_2\text{O}$ crystals (M^{2+} = divalent transition metal ion, $\text{X}^- = \text{Cl}^-$ or Br^-) are summarized (45-50). Except for $\text{CrCl}_2 \cdot 4\text{H}_2\text{O}$ and $\text{MnCl}_2 \cdot 4\text{H}_2\text{O}$, the chloride salts have the *cis*-form, whereas the bromide salts have the *trans*-form, again except for the manganese(II) bromide tetrahydrate crystal. The manganese(II) halides prefer the *cis*-form. On the other hand, the iron(II) halide salts prefer the *trans*-form. Although a satisfactory explanation has not been given for the *cis*-*trans* stereoselectivity in the transition metal halide salts, it is plausible that the hydrogen-bonding interactions between the halide ions in the complex unit and water molecules coordinated to

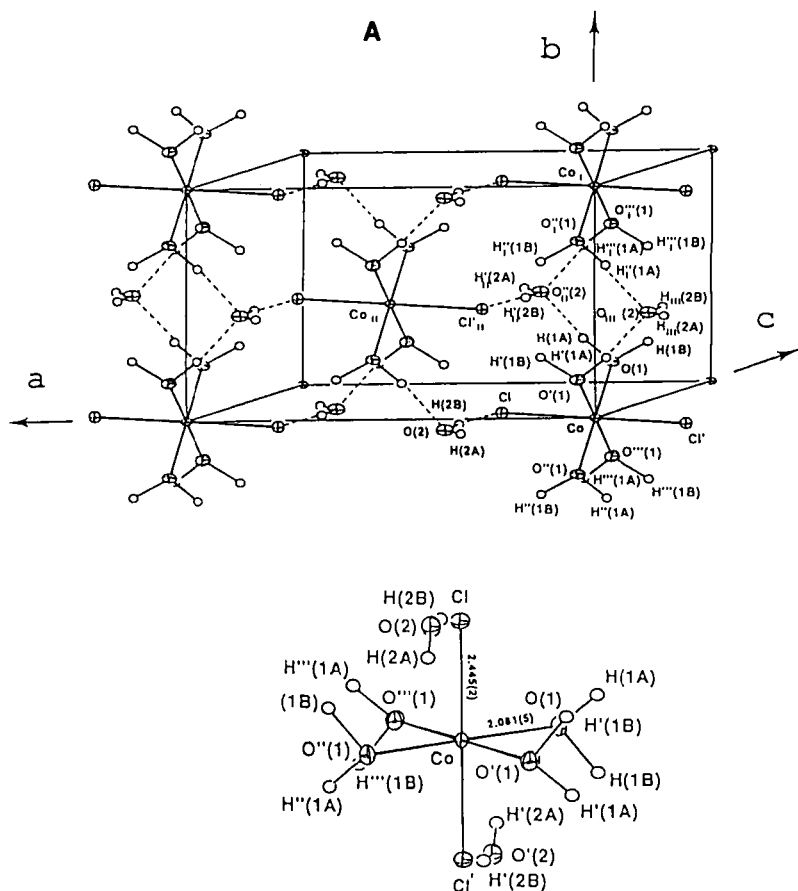
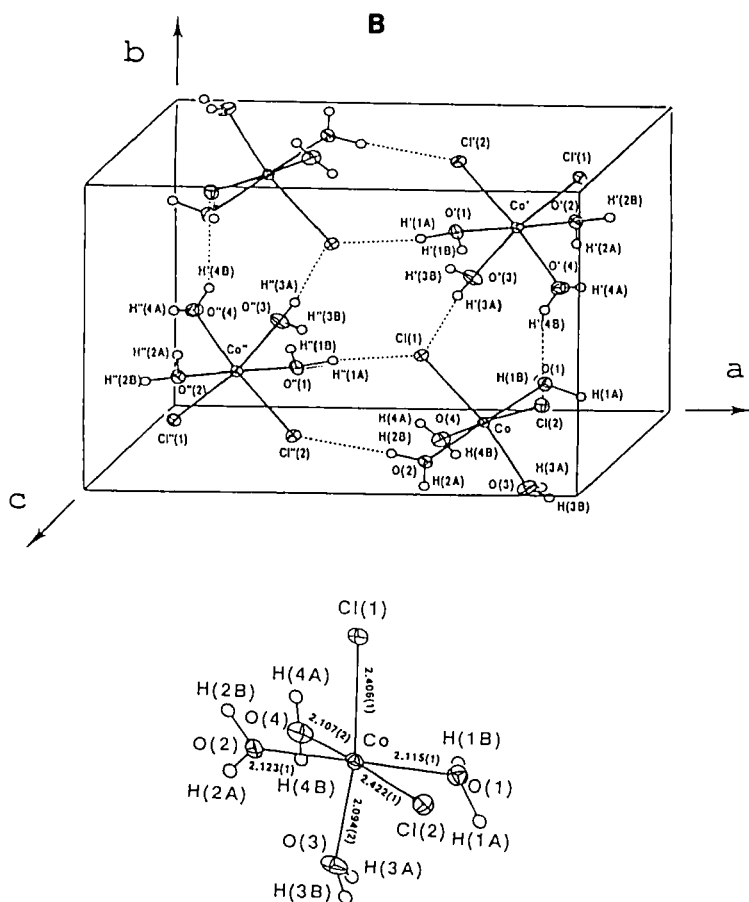


FIG. 8. ORTEP diagrams of crystal structures of (A) $\text{CoCl}_2 \cdot 6\text{H}_2\text{O}$, (B) $\text{CoCl}_2 \cdot 4\text{H}_2\text{O}$, and (C) $\text{CoCl}_2 \cdot 2\text{H}_2\text{O}$.

the metal ion in the adjacent complex unit may play an essential role in the *cis-trans* selectivity occurring in the solid phase.

B. WHY IS THE HYDRATE MELT OF $\text{CaCl}_2 \cdot R\text{H}_2\text{O}$ WITH $R = 6$ EASILY SUPERCOOLED BUT HYDRATE MELTS WITH $R = 4$ AND 8.6 ARE NOT?

Some liquids can be supercooled when the temperature is decreased. It is easily supposed that a liquid-solid equilibrium might be achieved quickly when the molecular arrangement of a liquid is similar to that in the solid, which should be in equilibrium with the liquid at the



melting point. For instance, dimethyl sulfoxide, whose liquid structure at 25°C is fairly similar to that of the solid state (51), has a sharp melting point that is only 6.6°C below room temperature, whereas water is easily supercooled and even forms a glass. Therefore, it is easily supposed that the similarity and dissimilarity in the structures of liquid and solid states of a substance might have a key role in the supercooling phenomenon.

A comparison between structures of calcium(II) chloride hydrate crystals and melts, which can be used as a heat storage material, has been carried out by means of X-ray diffraction (52). The phase diagram of

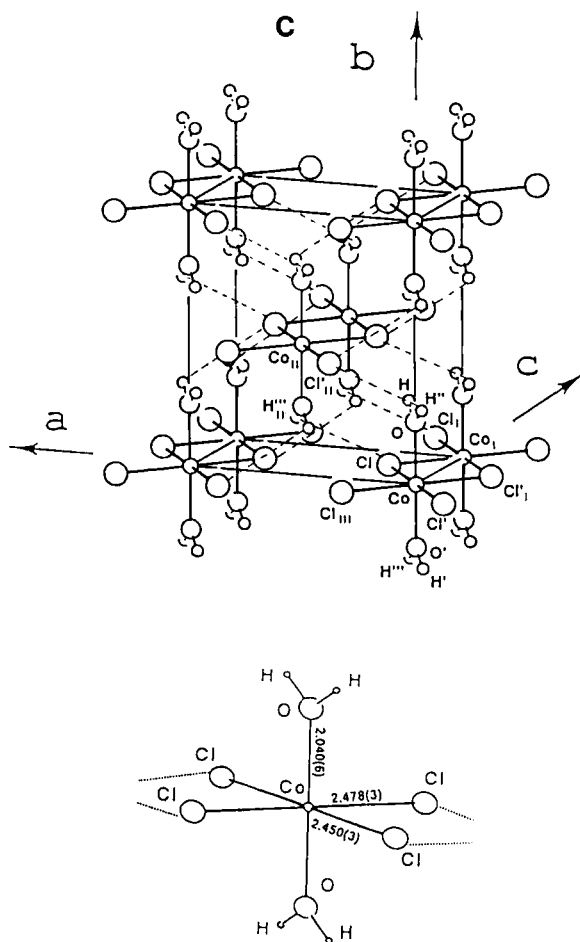


FIG. 8. (Continued)

calcium(II) chloride hydrates is shown in Fig. 9 over a composition range from 0 to 80 wt% in water and at temperatures from -60 to 220°C . In the composition range from 30 to 50 wt% CaCl_2 , $\text{CaCl}_2 \cdot 6\text{H}_2\text{O}$ forms as the solid. From ~ 50 to 55, $\alpha\text{-CaCl}_2 \cdot 4\text{H}_2\text{O}$ is the solid equilibrated with the hydrate melt. However, $\beta\text{-CaCl}_2 \cdot 4\text{H}_2\text{O}$ can be formed as a metastable solid at a slightly lower temperature as indicated by the broken line in Fig. 9. Another metastable $\gamma\text{-CaCl}_2 \cdot 4\text{H}_2\text{O}$ form is obtained at low temperatures. Thus, there are three peritectic points (two of them as shown in Fig. 9) and the melting point maximum in

TABLE V

INFORMATION ON THE STRUCTURES OF $\text{MX}_2 \cdot 4\text{H}_2\text{O}$ CRYSTALS, INCLUDING IONIC RADII OF THE METAL, HALIDE IONS, AND WATER MOLECULE r , AND LENGTHS $r_{\text{M-X}}$ AND $r_{\text{M-OH}_2}$ OF THE METAL-HALIDE AND METAL-WATER BONDS, RESPECTIVELY^a

Metal: r_{M} (pm):	Cr ²⁺ 80	Mn ²⁺ 82	Fe ²⁺ 78	Co ²⁺ 74.5	Ni ²⁺ 69	Cu ²⁺ 73
$\text{X}^- = \text{Cl}^-$						
Type	<i>trans</i>	<i>cis</i>	<i>trans</i>	<i>cis</i>	<i>cis</i>	—
$r_{\text{M-Cl}}$	275.8	247.5 250.0	252.6	240.6 242.2	237.4 239.7	
$r_{\text{M}} + r_{\text{Cl}}$	261	263	259	255.5	250	
$r_{\text{M-OH}_2}$	208.1 207.4	222.4 218.5 220.9 220.6	211.7 208.2	211.5 209.4 212.3 210.7	207.5 208.0 207.0 205.8	
$r_{\text{M}} + r_{\text{OH}_2}$	220	223	218	214.5	209	
Ref.	46	47	48	44	49	
$\text{X}^- = \text{Br}^-$						
Type	—	<i>cis</i>	<i>trans</i>	<i>trans</i>	—	<i>trans</i>
$r_{\text{M-Br}}$		262.9 265.2	266.82	261.9		308.2 242.6
$r_{\text{M}} + r_{\text{Br}}$		279	274	270.5		269
$r_{\text{M-OH}_2}$		221.8 217.6 221.6 219.1	211.2 207.7	206.1 206.8		193
$r_{\text{M}} + r_{\text{OH}_2}$		223	218	214.5		213
Ref.		50	49	49		49

^a The unit of bond length (pm). Ionic radii are quoted from Ref. (45).

the vicinity of the equilibrium lines of the tetra- and hexahydrates. At higher temperatures di- and monohydrates exist as the solid.

Hydrated melts with the composition $\text{CaCl}_2 \cdot R\text{H}_2\text{O}$ and $R = 4.0$ (A), 6.0 (B), and 8.6 (C) have been prepared at 120, 33, and 25°C, respectively. On cooling, the $\text{CaCl}_2 \cdot 4\text{H}_2\text{O}$ and $\text{CaCl}_2 \cdot 8.6\text{H}_2\text{O}$ hydrated melts form crystals of $\beta\text{-CaCl}_2 \cdot 4\text{H}_2\text{O}$ and $\text{CaCl}_2 \cdot 6\text{H}_2\text{O}$, respectively, but $\text{CaCl}_2 \cdot 6\text{H}_2\text{O}$ is easily supercooled without formation of crystals.

X-ray diffraction analysis of the structure of the hydrate melts reveals that the calcium(II) ion in the $\text{CaCl}_2 \cdot 8.6\text{H}_2\text{O}$ (25°C) is surrounded by six water molecules with a Ca-OH_2 distance of 245 pm (see Fig. 10). Chloride ions tend to enter the first coordination sphere of the calcium(II) with decreasing water concentration in the melt to form ion

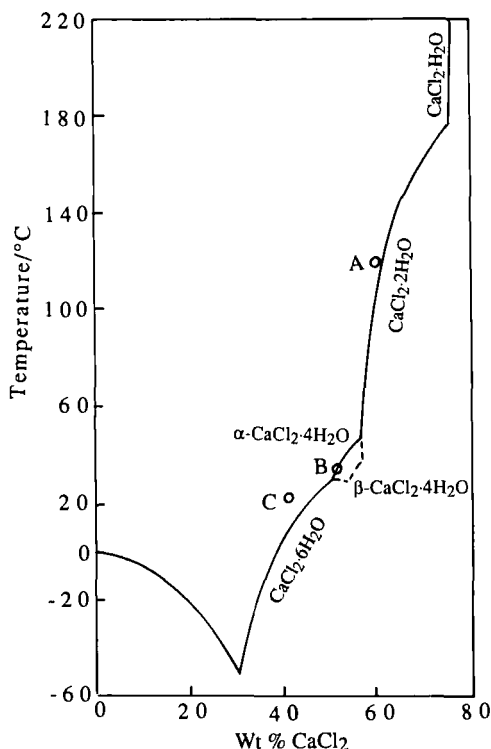
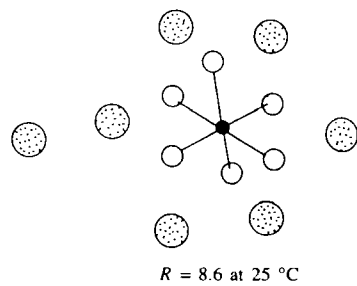
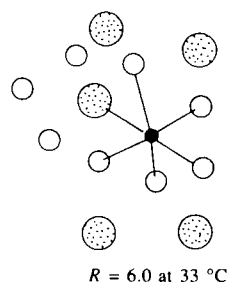
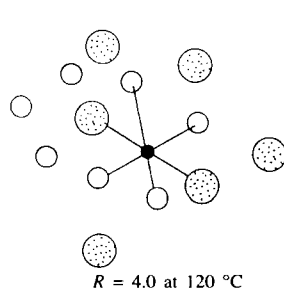


FIG. 9. The phase diagram of the $\text{CaCl}_2\text{-H}_2\text{O}$ system and composition of hydrate melts examined. (A) $\text{CaCl}_2\cdot 4\text{H}_2\text{O}$ at 120 $^{\circ}\text{C}$; (B) $\text{CaCl}_2\cdot 6\text{H}_2\text{O}$ at 33 $^{\circ}\text{C}$; (C) $\text{CaCl}_2\cdot 8.6\text{H}_2\text{O}$ at 25 $^{\circ}\text{C}$.

pairs with a $\text{Ca}^{2+}\text{-Cl}^-$ bond of 270 pm. In the $\text{CaCl}_2\cdot 6\text{H}_2\text{O}$ melt about one Cl^- ion binds to every calcium(II), whereas about two Cl^- ions are coordinated to one Ca^{2+} ion in the $\text{CaCl}_2\cdot 4\text{H}_2\text{O}$ melt. Interestingly, the coordination structure of the calcium(II) ion in $\text{CaCl}_2\cdot 6\text{H}_2\text{O}$ melt does not resemble the structure of $\beta\text{-CaCl}_2\cdot 4\text{H}_2\text{O}$, which is the solid in equilibrium with the melt. However, the structure of the calcium(II) ion in the $\beta\text{-CaCl}_2\cdot 4\text{H}_2\text{O}$ crystal is similar to that in the $\text{CaCl}_2\cdot 8.6\text{H}_2\text{O}$ melt (see Fig. 10), although the hydration number of the calcium(II) ion is larger in the crystal than in the $\text{CaCl}_2\cdot 8.6\text{H}_2\text{O}$ melt.

Thus, the supercooling phenomenon in the calcium(II) chloride hexahydrate melts may be explained in terms of the dissimilarity in the structure around the calcium(II) ions in the melt and in the crystal, and the substitution of water by chloride in the coordination sphere of the calcium(II) ion in the melt should be completed during cooling. On the other hand, the $\text{CaCl}_2\cdot 4\text{H}_2\text{O}$ hydrate melt has a very similar

Structure of Hydrate Melts



Structure in Crystal

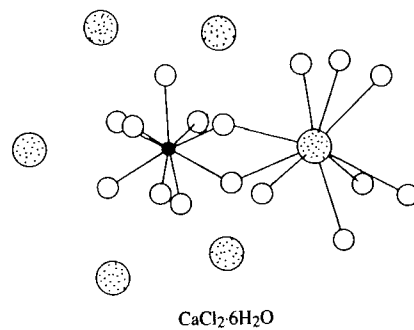
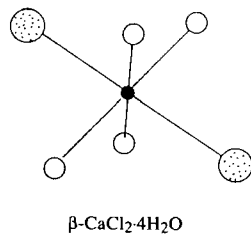


FIG. 10. The coordination structures around calcium ions in the hydrate melts and crystals. ●, Ca^{2+} ; ○, H_2O ; ⊙, Cl^- .

coordination of the calcium(II) to that of β - $\text{CaCl}_2 \cdot 4\text{H}_2\text{O}$, and a simple gathering of hydrated calcium(II) and chloride ions results in the construction of the crystal structure. In the case of the crystallization of the $\text{CaCl}_2 \cdot 8.6\text{H}_2\text{O}$ melt, more water molecules must be introduced into the first coordination sphere around the calcium(II). The reaction may however be diffusion controlled.

C. WHY DOES THE $\text{M}^{\text{I}}\text{Cl} \cdot \text{MgCl}_2 \cdot 6\text{H}_2\text{O}$ DOUBLE SALT FORM BY THE ADDITION OF A SMALL AMOUNT OF ALKALI METAL IONS M^{I} TO A MAGNESIUM(II) CHLORIDE SOLUTION BUT NOT IN THE REVERSE CASE?

Studies on double salts have been carried out mostly on the basis of phase diagrams of the different components and crystallographic structures. A number of studies have been carried out on the double salts of the type $\text{M}^{\text{I}}\text{X} \cdot \text{M}^{\text{II}}\text{X}_2 \cdot n\text{H}_2\text{O}$ with various combinations of M^{I} , M^{II} , and X. Solubilities and phase diagrams of the salts have been studied under various conditions, and a wide variety of X-ray crystallographic investigations have been reported in the literature.

Double salt problems are of practical importance in the chemical industry. However, only limited discussion has appeared concerning an elucidation of the mechanism of formation, because reliable information on the structure of ions in solution is not available. The development of solution X-ray diffraction and EXAFS techniques can throw new light on the problem to elucidate the mechanism of formation of double salts. As a case study we take a series of double salts $\text{M}^{\text{I}}\text{Cl} \cdot \text{MgCl}_2 \cdot n\text{H}_2\text{O}$, where M^{I} denotes an alkali metal or an ammonium ion.

Magnesium(II) chloride is highly soluble in water and the solid salt that is in equilibrium with the saturated aqueous solution exists as the hexahydrate $\text{MgCl}_2 \cdot 6\text{H}_2\text{O}$ at room temperature. At lower temperatures than -10°C magnesium(II) chloride forms the octa- and dodecahydrate crystals.

Magnesium(II) chloride forms double salts with various alkali chlorides. Lithium chloride forms $\text{LiCl} \cdot \text{MgCl}_2 \cdot 7\text{H}_2\text{O}$. However, the crystal structure of the salt has not been determined yet. Interestingly, no double salt of MgCl_2 with NaCl forms. Potassium chloride forms carnallite with magnesium(II) chloride, which has a composition $\text{KCl} \cdot \text{MgCl}_2 \cdot 6\text{H}_2\text{O}$. Ammonium, rubidium, and cesium also form double salts with magnesium(II) chloride having the same composition of $\text{M}^{\text{I}}\text{Cl} \cdot \text{MgCl}_2 \cdot 6\text{H}_2\text{O}$ as carnallite but the structure is of the perovskite type.

In crystals of $\text{M}^{\text{I}}\text{Cl} \cdot \text{MgCl}_2 \cdot 6\text{H}_2\text{O}$ ($\text{M}^{\text{I}} = \text{K}^+, \text{NH}_4^+, \text{Rb}^+, \text{Cs}^+$), the magnesium(II) ion is hexahydrated, and all of the monovalent cations

are coordinated by six chloride ions. The different crystal structures formed depend on the different ionic sizes of the M^I ions. The tolerance factor $t = (r_{M^I} + r_X) / \{\sqrt{2}(r_{M^{II}} + r_X)\}$ introduced by Goldschmidt (53) should be 0.80 to 1.00 for the formation of the perovskite-type structure, whereas the carnallite-type structure forms when t become larger than 1.00. From the above requirement, the radius of the $[\text{Mg}(\text{H}_2\text{O})_6]^{2+}$ ion has been evaluated as 290 pm, which is smaller than the sum 354 pm = (72 + 282) pm. The first term on the right-hand side of the equation is the crystallographic ionic radius of Mg^{2+} (54), and the second term is the diameter of a water molecule (55). The smaller size of $[\text{Mg}(\text{H}_2\text{O})_6]^{2+}$ thus compared with that calculated from the reported sizes of Mg^{2+} and H_2O shows that the $[\text{M}^I\text{Cl}_6]$ unit forms hydrogen bonds with water molecules in the coordination sphere of the magnesium(II) ion. The simple assumption that the ions are spherical does not hold therefore. In fact, a face of the small octahedron of $[\text{Mg}(\text{H}_2\text{O})_6]^{2+}$ and an edge of the large octahedron of $[\text{M}^I\text{Cl}_6]^{5-}$ practically contact each other in the crystal structure (Fig. 11) (56, 57).

Solution X-ray diffraction measurements for saturated aqueous solutions of the $\text{KCl} \cdot \text{MgCl}_2 \cdot 6\text{H}_2\text{O}$ and $\text{CsCl} \cdot \text{MgCl}_2 \cdot 6\text{H}_2\text{O}$ double salts at 25°C reveal that magnesium(II) ions in the solutions are fully hydrated as $[\text{Mg}(\text{H}_2\text{O})_6]^{2+}$ with a Mg–O bond length of 208–209 pm. This is essentially the same bond length as in the double salt crystals, and the K^+ and Cs^+ ions have both water molecules and chloride ions in their first coordination sphere. The coordination numbers for water molecules and chloride ions around a K^+ ion are 4.7 and 2.4, respectively, and those around a Cs^+ ion are 4.7 and 2.0, respectively. The $\text{K}^+ - \text{OH}_2$ and $\text{K}^+ - \text{Cl}^-$ interatomic distances are found to be 227 and 320 pm, respectively, and the $\text{Cs}^+ - \text{OH}_2$ and $\text{Cs}^+ - \text{Cl}^-$ distances are 315 and 339 pm, respectively (58). The interatomic distances determined are essentially the same as those that have been reported in the literature for aqueous solutions of potassium and cesium salts.

Potassium and cesium ions form chloro complexes in the saturated aqueous solutions of the $\text{KCl} \cdot \text{MgCl}_2 \cdot 6\text{H}_2\text{O}$ and $\text{CsCl} \cdot \text{MgCl}_2 \cdot 6\text{H}_2\text{O}$ double salts, which contain much more chloride than a saturated alkali chloride salt solution because of the high solubility of MgCl_2 . Moreover 2 mol of chloride are liberated from 1 mol of the salt, and the hydrated water molecules of potassium and cesium ions are partly substituted with chloride to form $[\text{M}^I\text{Cl}_x(\text{H}_2\text{O})_y]^{(1-x)+}$ complexes, which are easily converted to $[\text{M}^I\text{Cl}_6]^{5-}$ on formation of crystals. Thus, in a saturated magnesium(II) chloride aqueous solution the magnesium(II) ion is fully hydrated to form $[\text{Mg}(\text{H}_2\text{O})_6]^{2+}$ and all chloride ions are weakly hydrated in the solution. Upon addition of a minute amount of M^ICl

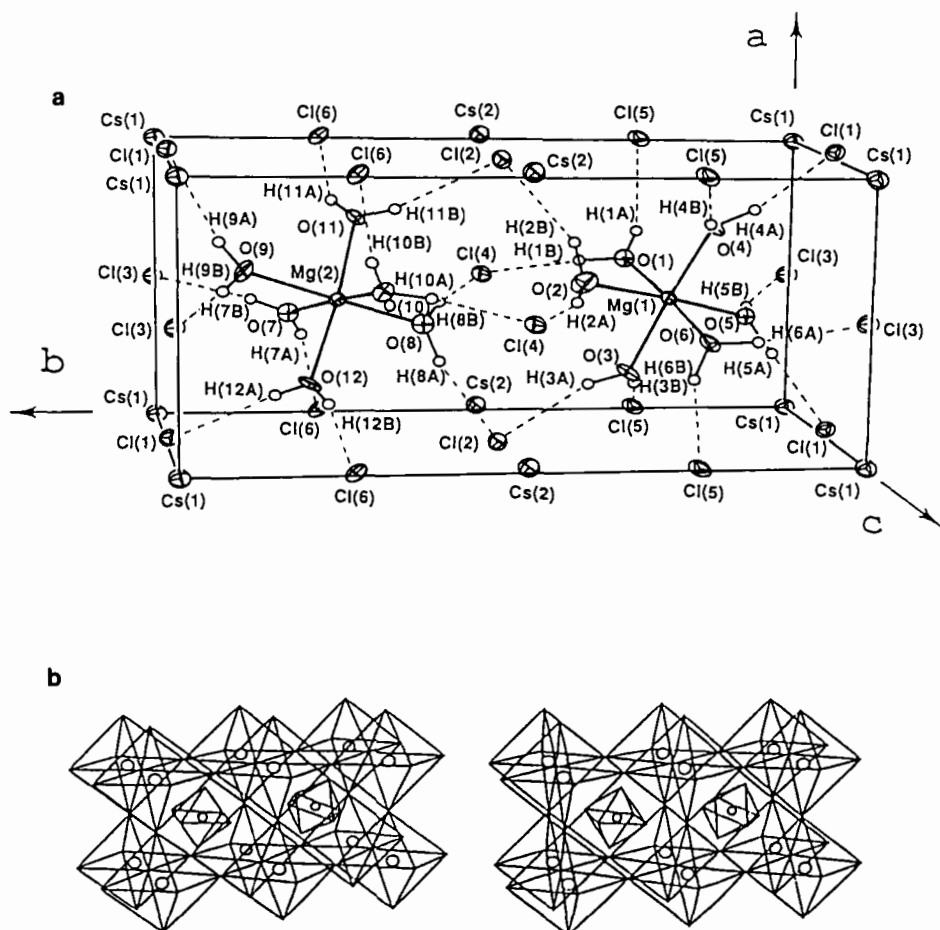


FIG. 11. The structure of $\text{CsCl} \cdot \text{MgCl}_2 \cdot 6\text{H}_2\text{O}$ crystal. (a) ORTEP drawing with the thermal ellipsoids scaled at the 30% probability level; hydrogen atoms are represented by dashed lines. (b) Stereoscopic drawing, with large and small octahedra representing $[\text{CsCl}_6]^{5-}$ and $[\text{Mg}(\text{H}_2\text{O})_6]^{2+}$ units, respectively.

($\text{M}^I = \text{K}^+, \text{NH}_4^+, \text{Rb}^+, \text{and Cs}^+$) the hydrated M^I ions are partially coordinated with chloride ions, water molecules may be easily replaced with chloride ions to form $[\text{M}^I\text{Cl}_6]^{5-}$ as a part of the crystal formation process, because the $\text{M}^I\text{-OH}_2$ bond is rather weak. The rate constant for substitution may be in the order of 10^8 s^{-1} , which is the rate constant for replacement of a hydrated water molecule of the alkali metal ion (59). Since the rate of formation of clusters from hydrated magnesium(II) ions and partially hydrated chloro complexes of alkali metal

ions may be diffusion controlled (21), the rate of formation of crystal nuclei may be determined by the rate of the substitution of hydrated water molecules with chloride ions.

When a small amount of magnesium(II) ions in a saturated solution of an alkali chloride is added, no double salt is formed and each component ion exists as the hydrated species. In saturated aqueous solutions of alkali chloride, only 1:1 ion pairs are formed and no highly coordinated species like $[M^I Cl_x (H_2O)_y]^{(1-x)+}$ ($x > 1$) are formed (26) except for CsI (31, 34), in which case both the cation and the anion are the most weakly hydrated among the alkali metal and halide ions, respectively. Such highly coagulated polynuclear complexes can be formed in super-saturated solutions (26). The chloride concentration in the saturated solution is not high enough to form $[M^I Cl_x (H_2O)_y]^{(1-x)+}$ ($x > 1$) complexes, and $[M^I Cl_6]$ species are not formed extensively in solution. Thus, $M^I Cl \cdot MgCl_2 \cdot 6H_2O$ crystals cannot be formed even though Mg^{2+} ions are coexisting with a large amount of $M^I Cl$.

VII. Concluding Remarks

The dissolution and formation of crystals are well-known phenomena. Despite this, knowledge of the mechanism at a molecular level is extremely limited. Besides studies by classical methods and macroscopic observations, modern techniques involving solution X-ray and neutron diffraction and EXAFS methods are used to determine the structure of the component species in the solution phase. In addition, studies on the solid phase and computer simulations that elucidate microscopic, static, and dynamic structures of the reacting species in solutions are being applied in order to investigate the dissolution and nucleation processes. Furthermore, the observation of crystal formation and growth from nuclei can be achieved with the aid of high-speed computers and graphic displays. The development of ultra-high-speed computers is expected to make possible the simulation of reasonably large systems and help in the further understanding of such phenomena.

ACKNOWLEDGMENTS

This work has been financially supported, in part, by Grants-in-Aid for Scientific Research on Priority Area "Molecular Approaches to Non-equilibrium Processes in Solutions" (No. 02245106 and No. 03231105) from the Ministry of Education, Science and

Culture, Japan. Computers at the Institute for Molecular Science and Fujitsu Co. were used. Video pictures were prepared using a program for graphic displays available from the Fujitsu Co.

REFERENCES

1. N. Bjerrum, *Mat.-Fiz. Medd.—K. Dan. Vidensk. Selsk.* **21**, 1 (1951).
2. A. Ben-Naim and F. H. Stillinger, in "Water and Aqueous Solutions" (Horne, R. A., ed.), p. 159. Wiley (Interscience), New York, 1979.
3. F. H. Stillinger, and A. Rahman, *J. Chem. Phys.* **60**, 1545 (1974).
4. J. S. Rowlinson, *Trans. Faraday Soc.* **47**, 120 (1951).
5. O. Matsuoka, E. Clementi, M. Yoshimine, *J. Chem. Phys.* **64**, 1351 (1976).
6. V. Carravetta, and E. Clementi, *J. Chem. Phys.* **81**, 2646 (1984).
7. R. O. Watts, *Chem. Phys.* **26**, 367 (1977).
8. H. L. Lemberg, and F. H. Stillinger, *J. Chem. Phys.* **62**, 1677 (1975).
9. A. Rahman, F. H. Stillinger, and H. L. Lemberg, *J. Chem. Phys.* **63**, 5223 (1975).
10. F. H. Stillinger, and A. Rahman, *J. Chem. Phys.* **68**, 666 (1978).
11. P. Bopp, G. Jancó, and K. Heinzinger, *Chem. Phys. Lett.* **89**, 129 (1983).
12. M. D. Morse, and S. A. Rice, *J. Chem. Phys.* **76**, 650 (1982).
13. H. Kistenmacher, H. Popkie, and E. Clementi, *J. Chem. Phys.* **59**, 1325 (1973).
14. G. Pálincás, W. O. Riede, and K. Heinzinger, *Z. Naturforsch., A* **32**, 1137 (1977).
15. F. G. Fumi, and M. P. Tosi, *J. Phys. Chem. Solidis* **25**, 31 (1964); M. P. Tosi, and F. G. Fumi, *ibid.* p. 45.
16. K. Heinzinger, in "Computer Modelling of Fluids, Polymers and Solids" (C. R. A. Catlow, S. C. Parker, and M. P. Allen, eds.), p. 357. Kluwer Academic Publ., New York, 1990.
17. P. P. Ewald, *Ann. Phys. (Leipzig)* [4] **64**, 253 (1921).
18. H. Ohtaki, N. Fukushima, E. Hayakawa, and I. Okada, *Pure Appl. Chem.* **60**, 1321 (1988).
19. H. Ohtaki, and N. Fukushima, *Pure Appl. Chem.* **61**, 179 (1989).
20. N. Fukushima, Y. Tamura, and H. Ohtaki, *Z. Naturforsch., A* **46**, 193 (1991).
21. H. Ohtaki, and N. Fukushima, *Pure Appl. Chem.* **63**, 1743 (1991).
22. R. F. Kruh, *Chem. Rev.* **62**, 319 (1962).
23. H. Ohtaki, *Rev. Inorg. Chem.* **4**, 103 (1962).
24. Y. Marcus, *Chem. Rev.* **88**, 1475 (1988).
25. M. Magini, ed., "X-Ray Diffraction of Ions in Aqueous Solutions: Hydration and Complex Formation." CRC Press, Boca Raton, FL, 1988.
26. H. Ohtaki, and N. Fukushima, *J. Solution Chem.* **21**, 23 (1991).
27. Copies of video tapes for scientific and educational purposes are available on request at a small charge to cover the cost of cassettes and copying.
28. P. Bopp, I. Okada, H. Ohtaki, and K. Heinzinger, *Z. Naturforsch., A* **40**, 116 (1985).
29. T. Tanaka, N. Ogita, Y. Tamura, I. Okada, H. Ohtaki, G. Pálincás, E. Spohr, and K. Heinzinger, *Z. Naturforsch., A* **42**, 29 (1987).
30. A. P. Copestake, G. W. Neilson, and J. E. Enderby, *J. Phys. C* **18**, 4211 (1985).
31. Y. Tamura, T. Yamaguchi, I. Okada, and H. Ohtaki, *Z. Naturforsch., A* **42**, 367 (1987).
32. Deleted in proof.
33. Gy. I. Szász, and K. Heinzinger, *Z. Naturforsch., A* **38**, 214 (1983).

34. Y. Tamura, H. Ohtaki, and I. Okada, *Z. Naturforsch.*, A **46**, 1083 (1991).
35. H. Ohtaki, and N. Fukushima, *Pure Appl. Chem.* **93**, 1743 (1991).
36. D. L. Wertz, and R. F. Kruh, *J. Chem. Phys.* **50**, 4313 (1969).
37. M. Magini, *J. Chem. Phys.* **74**, 2523 (1981).
38. H.-G. Lee, Y. Matsumoto, T. Yamaguchi, and H. Ohtaki, *Bull. Chem. Soc. Jpn.* **56**, 443 (1983).
39. G. Paschina, G. Piccaluga, G. Pinna, and M. Magini, *Chem. Phys. Lett.* **98**, 157 (1983).
40. A. Musinu, G. Paschina, G. Piccaluga, and M. Magini, *J. Chem. Phys.* **80**, 2772 (1984).
41. J. Bjerrum, A. S. Halonin, and L. H. Skibsted, *Acta Chem. Scand., Ser. A* **29**, 326 (1975).
42. L. H. Skibsted, and J. Bjerrum, *Acta Chem. Scand., Ser. A* **32**, 429 (1978).
43. L. G. Sillén, and A. E. Martell, eds., "Stability Constants of Metal-Ion Complexes," Spec. Publ. No. 17, Suppl. No. 1. Chem. Soc., London, 1964; Spec. Publ. No. 25 (1971).
44. K. Waizumi, H. Masuda, H. Ohtaki, K. Tsukamoto, and I. Sunagawa, *Bull. Chem. Soc. Jpn.* **63**, 3426 (1990).
45. R. Shannon, *Acta Crystallogr., Sect. A* **32**, 751 (1976).
46. H. G. von Schnering, and B.-H. Brand, *Z. Anorg. Allg. Chem.* **402**, 159 (1973).
47. Z. M. El Saffar, and G. M. Brown, *Acta Crystallogr., Sect. B* **27**, 66 (1971).
48. P. J. Meunier-Piret, and M. van Meerssches, *Acta Crystallogr., Sect. B* **28**, 2329 (1972).
49. K. Waizumi, H. Masuda, and H. Ohtaki, *Inorg. Chim. Acta* **192**, 173 (1992).
50. E. D. Crozier, and N. Alberding, *Acta Crystallogr., Sect. C* **39**, 808 (1983).
51. S. Itoh, and H. Ohtaki, *Z. Naturforsch.*, A **42**, 858 (1987).
52. T. Yamaguchi, S. Hayashi, and H. Ohtaki, *Inorg. Chem.* **28**, 2434 (1989).
53. V. M. Goldschmidt, "Geochemische Verteilungsgesetze der Elemente, VII," Sk. Nor. Vidensk.-Akad., Oslo, 1926.
54. R. D. Shannon, *Acta Crystallogr., Sect. A* **32**, 751 (1976).
55. A. Ben-Naim, "Water and Aqueous Solutions." Plenum, New York, 1974.
56. K. Waizumi, H. Masuda, H. Ohtaki, K. Burkov, and M. Y. Scripkin, *Acta Crystallogr. Sect. C* **47**, 251 (1991).
57. K. Waizumi, H. Masuda, and H. Ohtaki, *Am. Mineral.* **76**, 1864 (1991).
58. K. Waizumi, Y. Tamura, H. Masuda, and H. Ohtaki, *Z. Naturforsch.*, A **46**, 307 (1990).
59. M. Eigen, *Ber. Bunsenges. Phys. Chem.* **67**, 753 (1963).